Original Paper

Effect of modification degrees on the interfacial properties and EOR efficiency of amphiphilic Janus graphene oxide

Han Jia [a, b, *], Xin Wei [a, b], Qiu-Xia Wang [c], Yuan-Bo Wang [a, b], Shi-Jie Wen [a, b], Fang-Ning Fan [a, b], Qiang Wang [a, b], Zhe Wang [a, b], De-Xin Liu [a, b], Pan Huang [d, **]

[a] Key Laboratory of Unconventional Oil & Gas Development (China University of Petroleum (East China)), Ministry of Education, Qingdao, Shandong 266580, China
[b] Shandong Key Laboratory of Oilfield Chemistry, School of Petroleum Engineering, China University of Petroleum (East China), Qingdao, Shandong 266580, China
[c] Bohai Oilfield Research Institute, Tianjin Branch, CNOOC China Limited, Tianjin 300459, China
[d] Department of Chemical and Materials Engineering, University of Alberta, Edmonton AB T6G 1H9, Canada

ARTICLE INFO

ABSTRACT

Asymmetrically modified Janus graphene oxide (JGO) has attracted great attention due to its unique physical chemistry properties and wide applications. The modification degree of Janus nanosheets inevitably affects their interfacial activity, which is essential for their performances in enhanced oil recovery (EOR). In this study, the interfacial properties of Janus graphene oxide (JGO) with various modification degrees at liquid-liquid and liquid-solid interfaces were systematically evaluated via the measurements of interfacial tension (IFT), dilatational modulus, contact angle, and EOR efficiency was further assessed by core flooding tests. It is found that JGO-5 with higher modification degree exhibits the greater ability to reduce IFT (15.16 mN/m) and dilatational modulus (26 mN/m). Furthermore, JGO can construct interfacial and climbing film with the assistance of hydrodynamic power to effectively detach the oil from the rock surface and greatly enhance oil recovery. Moderately modified JGO-2 can highly improve recovery of residual crude oil (11.53%), which is regarded as the promising EOR agent in practical application. The present study firstly focuses on the effects of modification degrees on the JGO interfacial properties and proposes diverse EOR mechanisms for JGO with different modification degrees.
© 2022 The Authors. Publishing services by Elsevier B.V. on behalf of KeAi Communications Co. Ltd. This is an open access article under the CC BY-NC-ND license (http://creativecommons.org/licenses/by-nc-nd/4.0/).

1. Introduction

In recent years, nanofluid displacement technology has attracted extensive attention in the oil and gas upstream industry (Alnarabiji et al., 2018; Jia et al., 2021a, b; Pal and Mandal, 2020a; Sikiru et al., 2021; Suleimanov et al., 2011; Sun et al., 2017; Tian et al., 2021; Toda et al., 2015; Zhao et al., 2018). The nanoparticles, whose sizes delicately match with the formation nanopores, can deeply penetrate into the pore-throat (Ali et al., 2020, 2021; Maurya and Mandal, 2016; Zhang and An, 2018). Then nanoparticles spontaneously adsorb at the rock surface to generate

structural disjoining pressure and alter rock surface properties, leading to the highly enhanced recovery of residual oil (Al-Anssari et al., 2016, 2017; Fang et al., 2016; Giraldo et al., 2019; Maurya and Mandal, 2018; Wei et al., 2017; Yin et al., 2019; Zhang et al., 2018).

Graphene oxide (GO) nanosheets are the products of chemical oxidation shedding of graphite powder (Shamaila et al., 2016), which has been widely investigated as a novel nanofluid displacement agent for EOR due to its fabulous physicochemical properties (Cao et al., 2022; de Vasconcelos et al., 2022; Jafarbeigi et al., 2020; Periasamy et al., 2017; Yoon et al., 2013). Barrabino et al. evaluated the potential of GO as a CO_2-based foam stabilizer to improve oil recovery (Barrabino et al., 2018). Liu et al. demonstrated that GO could be an efficient demulsifier for heavy oil-in-water emulsions (Liu et al., 2015). Although the GO nanosheets exhibit remarkable properties in many fields, their poor interfacial activity caused by the excessive hydrophilicity seriously restricts their potential applications. There are a considerable number of active

* Corresponding author. Key Laboratory of Unconventional Oil & Gas Development (China University of Petroleum (East China)), Ministry of Education, Qingdao, Shandong 266580, China.
** Corresponding author.
E-mail addresses: jiahan@upc.edu.cn (H. Jia), phuang4@ualberta.ca (P. Huang).

function groups with high chemical reactivity (epoxy group, hydroxy, carboxyl, and carbonyl groups) at the surface of GO nanosheets (Dimiev and Tour, 2014; Dreyer et al., 2010; Shams et al., 2019). Then the chemical modification of GO should be a feasible approach to solve the problem (Chen et al., 2021; Kumar et al., 2019; Lonkar et al., 2015; Wang et al., 2012, 2020; Zeng et al., 2020; Zhang et al., 2019).

Many literatures reported the symmetric modification of GO nanosheets could significantly improve their specific properties, such as heavy mental adsorption capacity (Sherlala et al., 2018), catalytic performance (Pei et al., 2021), and amphiphilicity regulation (Wu et al., 2015). Zhang et al. investigated the mechanisms of the improved thermal and mechanical performances of idealized GO modified by poly (dopamine) through molecular dynamics simulation (Zhang et al., 2021). Tadjarodi et al. designed a novel adsorbent of 2-pyridinecarboxaldehyde thiosemicarbazone modified GO to remove the mercury (II) from aqueous solutions (Tadjarodi et al., 2016).

Recently, researchers proposed and demonstrated the unique advantage of the asymmetrically modified GO (Ng et al., 2018). The heterogenous wetting distribution of asymmetric nanomaterials greatly enhanced their ability to bind to the interface (Tohidi et al., 2022). Furthermore, the amphiphilicity of nanosheets can be purposively adjusted to further promote their interfacial properties. Luo et al. first discovered that asymmetrically modified amphiphilic Janus graphene oxide (JGO) could self-assemble at the oil-water interface to fabricate a solid-like film (Luo et al., 2016, 2017). They suggested that the interfacial film formed by JGO could displace oil via piston-like oil displacement to achieve excellent EOR performance. Chen et al. reported that the high ability of JGO to stabilize the emulsion and induce wettability alteration for EOR in ultra-low permeability reservoirs (Luo et al., 2017). Lv et al. employed JGO as a shale inhibitor to reduce the filtration loss, which was attributed to its spontaneous adsorption at clay surface (Lv et al., 2020).

Previous literatures primarily concentrated on the JGO nanosheets with a single degree of modification to explore their performances and mechanisms. The modification degrees of JGO nanosheets will inevitably affect their interfacial activity, wettability, adsorption, and other properties. Our group synthesized various JGO nanosheets with different modification degrees and found their discrepant colloid stability in aqueous solutions (Huang et al., 2021). Then we attempt to explore the influence of chemical grafting degrees and the relative amphiphilicity on the interfacial properties of JGO nanosheets and their EOR efficiency, which is scarcely reported (from our knowledge).

In this work, a series of JGO with different modification degrees were synthesized and characterized via UV-vis spectra, X-ray photoelectron spectroscopy (XPS) analysis, and transmission electron microscope (TEM). Then dynamic interfacial tension, dilatational rheological, and contact angle measurements were performed to investigate the interfacial properties of JGO. Based on the results of core flooding tests, the diverse EOR mechanisms of JGO nanosheets with different modification degrees were proposed.

2. Experimental

2.1. Materials

Ethanol (> 99.7%), dodecylamine (> 98%), NaCl (> 99.5%), paraffin wax which melting point is around 59 $^\circ$C, and chloroform (> 99%) were brought from Shanghai Aladdin Biochemical Technology Co., Ltd., China. Graphene oxide was purchased from Turing Evolution Technical Company, China. The crude oil was obtained from the Daqing Oil Field.

2.2. Synthesis of JGO with various modification degrees

A series of dodecylamine modified JGO with different modification degrees were prepared based on the method (Pickering emulsion template) mentioned in the report of Huang et al. (2021). And the synthesis of JGO with different modifications were controlled by adjusting the proportion of dodecylamine to GO nanosheets. Detailed procedures of the modification process could be found in Supplementary Material. The obtained samples were identified from JGO-1 to JGO-5 with the increasing modification degrees.

2.3. Characterization of JGO

Cary 8454 UV-spectrophotometer (Agilent, USA) was employed to display the UV-vis spectra of samples. The XPS analysis (Thermo Scientific Escalab 250Xi, USA) was utilized to quantificationally calculate the grafting rates of dodecylamine at JGO surface. After that, the signal fitting software of XPSPEAK Version 4.1 was used to draw GO and JGO C1s fitting peaks. The sample morphologies in their aqueous solutions were observed by JEOL JEM-1400 transmission electron microscope (Japan). The zeta potential of GO and JGO in aqueous dispersion was measured by Malvern Zetasizer Nano ZS (Malvern, UK).

2.4. Interfacial tension and interfacial rheology tests

A dynamic interfacial oscillatory drop tensiometer (Tracker, Teclis, France) was used to detect the interfacial properties of GO and JGO, including IFT and interfacial rheology. The inverted needle was prepared to inject the octane droplet (20 μL) into the GO or JGO aqueous solutions. And a syringe was attached to a mechanical system oscillating in a sinusoidal wave to alter volume of the oil droplet. The IFT of the droplet could be reflected by its sinusoidal variation volume recorded by camera. Therefore, the Laplace-Young equation was utilized to acquire the IFT of octane droplet. Moreover, the dilatational modulus (E) is calculated using the following equation (Kovalchuk et al., 2019):

$$E = \frac{d\gamma}{d\ln A} \tag{1}$$

where γ is the interfacial tension (mN/m), A is the interface area (m^2).

The relationship among E, E' (elastic modulus), and E'' (viscous modulus) could also be represented in the plural form:

$$E = E' + iE'' = E' + i\omega\eta_d \tag{2}$$

where ω is the interfacial dilatation frequency, η_d is the interfacial dilatation viscosity.

For a viscoelastic interface, there is a phase angle (θ) between the sinusoidal variation of IFT and sinusoidal variation of interface area. E' and E'' can be calculated with E and θ by the following equations:

$$E' = E \cos(\theta) \tag{3}$$

$$E'' = E \sin(\theta) \tag{4}$$

2.5. Contact angle measurements

The contact angle goniometer (JC2000D5M, Zhongchen, China)

was utilized to access the contact angles. The sand stone was cut into slabs and soaked in crude oil for one week to obtain the oil-wet slabs (detailed procedures in Supplementary Material). The slab was taken directly from the crude oil, followed by hand shaking to remove the oil at surface. Then, the slab was placed in the rectangular glass cell filled with 20 mL GO or JGO aqueous solutions. A small crude oil droplet was naturally dripped to the slab surface, and the image of the oil droplet surface at the intersection point was captured to reflect the contact angle.

2.6. Core flooding tests

The properties of artificial cores were summarized in Table S1. The oil was the mixture of crude oil from Daqing Oil Field and white oil, with the viscosity of 9.8 mPa·s. The concentration of GO or JGO was 50 mg/L. The core flooding test was conducted with the subsequent operations: 1) the dried core was vacuumed in a core holder and then saturated with deionized (DI) water; 2) the oil was pumped into the core before the water cut fell below 1%; 3) DI water was injected up to the water cut above 98%; 4) 0.75 PV GO or JGO nanofluids was injected; 5) the injection was stopped with a soaking time of 12 h; 6) DI water was injected again until no oil was displaced.

3. Results and discussion

3.1. Characterization of JGO

Fig. 1 presents the UV-vis spectra of GO and JGO with different degrees of modification. It is obvious that both GO and JGO have two typical absorption peaks at 232 nm and 302 nm, which are ascribed to the π-π^* transition of $C=C$ and the n-π^* transition of $C=O$, respectively (Xiao et al., 2013). The higher energy for the electron transition of $C=C$ should be responsible for the greater absorption peak at 232 nm. The increased modification degrees hardly change the positions of both peaks but distinctly decrease their intensity. The chemical grafting of dodecylamine at the JGO surface results in the reduction of $C=C$ in GO. In addition, the reaction between dodecylamine and carboxyl group causes a slightly decreased number of $C=O$.
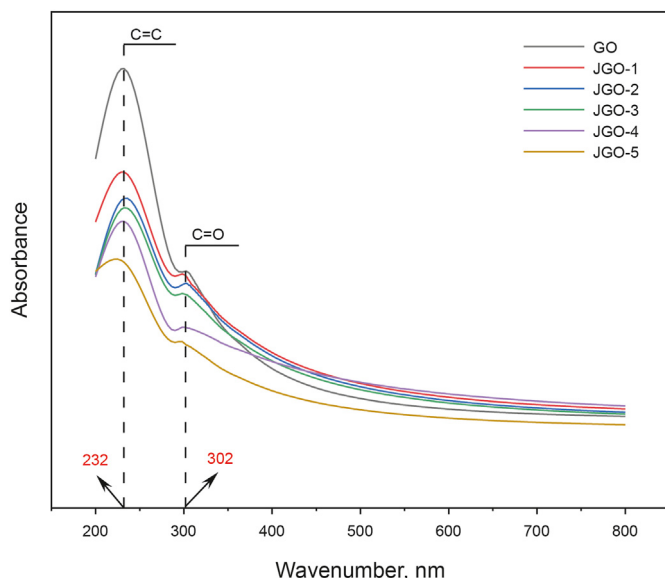

Fig. 1. UV-vis spectra of GO and JGO.

The measurement of UV-vis spectra can qualitatively confirm the different modification degrees of JGO. XPS analysis is further applied to distinguish the specific chemical composition of JGO and quantify the grafting ratios of dodecylamine at GO surface. As shown in Fig. 2a, there are five fitted peaks obtained from the C 1s signal of GO, which correspond to 284.8 eV (C−C), 286.2 eV (C−OH), 286.8 eV (C−O−C), 287.6 eV (C=O), 289.0 eV (O−C=O). Meanwhile, the slight deviation of binding energy for each chemical bond from GO to JGO-5 should be attributed to the recovering of the sp^2 network (Li et al., 2011). In addition, the presence of C−N peak (Liu et al., 2012) in all JGO samples indicates that dodecylamine reacted with the epoxy group at the GO surface. The percentage occupied by C−O−C, C−OH, and C−N in the plot is equal to the proportion of individual peak area of a single group to the sum of the areas covered by each group (Table 1). It is calculated that the gradually increased rates of C−OH and C−N against the proportion of C−O−C from JGO-1 to JGO-5, further verifying that the decrease in the number of epoxy groups at the surface is triggered by the ring-opening reaction. The conjunction ratios of dodecylamine at JGO surface are 0.0643 (JGO-1), 0.198 (JGO-2), 0.301 (JGO-3), 0.426 (JGO-4), and 0.498 (JGO-5).

Moreover, the TEM images reflect the similar morphologies of GO and JGO in their aqueous solutions (Fig. S1). The monodispersity of GO nanosheets is great, whereas the slight aggregates of JGO should be attributed to their increased hydrophobicity. The introduction of dodecylamine evidently decreases the absolute values of the zeta potential of the samples (Fig. S3), which is attributed to the alkyl chain shielding the ionization of oxygen-containing group on the nanosheets. While the absolute values of the zeta potential of all samples are greater than 35 mV, reflecting their favorable stability.

3.2. Effects of modification degrees on the interfacial properties of JGO

The interfacial properties of JGO are crucial for its application in improving oil recovery, which could be inevitably affected by the modification degrees. The octane-sample aqueous solution IFT and the dilatational interfacial rheology are shown in Fig. 3. JGO with higher modification degrees exhibits greater IFT reduction ability, indicating that higher content of dodecylamine grafted on JGO imparts it stronger amphiphilicity (Fig. 3a). However, the dilatational modulus (E) of the interface decreases obviously with increased modification degrees. Furthermore, the oil-water interface in the JGO system becomes more viscous, which is demonstrated by the ever-larger viscous modulus and phase angle from GO to JGO-5 (Fig. 3b). The largest E of GO system is ascribed to the generated rigid GO film at the interface (Fig. 3c). The E reduction from GO to JGO-5 can be interpreted from two aspects: 1) E is defined as the ratio of interfacial tension gradient ($d\gamma$) to interface area gradient ($dlnA$), and JGO with superior amphiphilicity can adsorb at oil-water interface to rapidly and greatly reduce $d\gamma$, which causes the lower E value (Maurya et al., 2017); 2) JGO can construct film at the interface, JGO-5 for instance (Fig. 3c), but with less rigidness than GO film. The adsorbed nanosheets at the interface overlap each other. The hydrogen-bond and π-π interaction between the overlapped parts of GO reinforce the GO interfacial film, whereas the overlapped parts of JGO may be relatively loosen due to the hindrance of dodecylamine. Thus, the JGO film is easy to deform, resulting in lower E and more distinct viscous features.

The adsorption of GO and JGO at the oil-water interface with increased hydrodynamic power is depicted in Fig. 4. Initially, the oil-water interface is concave due to the high octane-water IFT. There are no obvious changes for the interface in GO and JGO-1 system after shaking for one time. However, the adsorption of
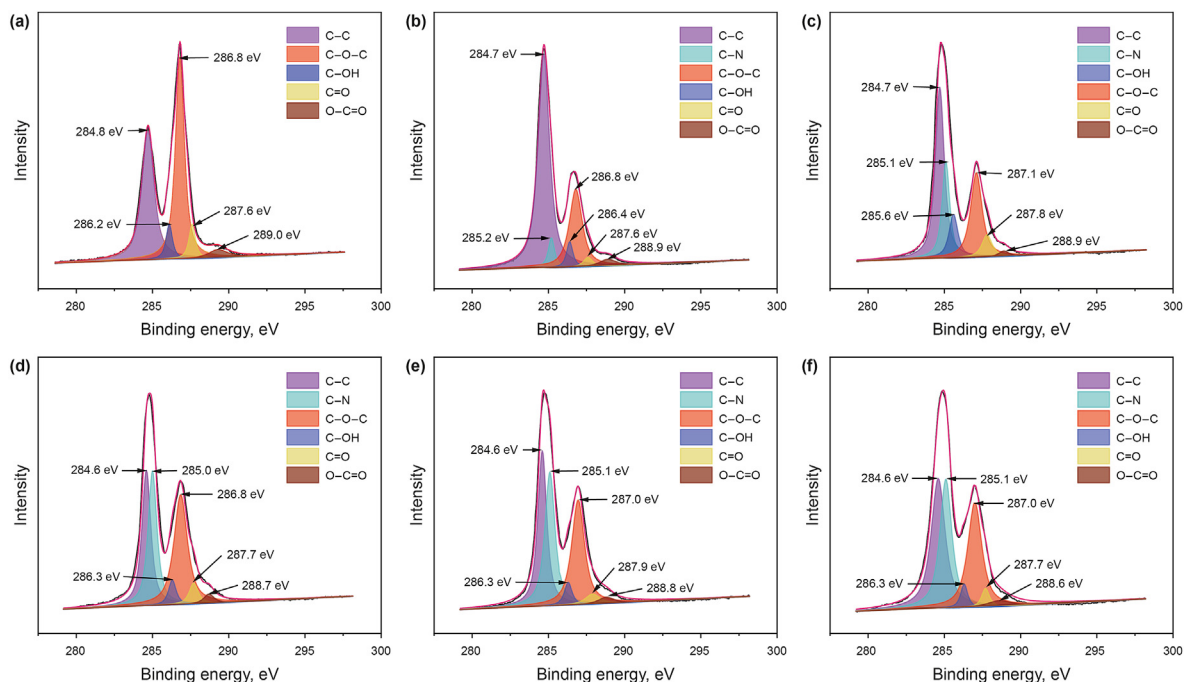
Fig. 2. XPS analysis of GO (**a**), JGO-1 (**b**), JGO-2 (**c**), JGO-3 (**d**), JGO-4 (**e**), and JGO-5 (**f**).

Table 1
Relative percentage of the integrated area of fitted peaks in GO and JGO.

Peak type	GO, %	JGO-1, %	JGO-2, %	JGO-3, %	JGO-4, %	JGO-5, %
C−O−C	59.63	36.84	33.24	29.43	24.35	19.83
C−OH	5.43	6.53	9.15	9.83	10.24	12.37
C−N	0	6.43	19.78	30.11	42.62	49.82

JGO with higher amphiphilicity evidently decrease the curvature of the oil-water interface (Jeon et al., 2019; Luo et al., 2016). Increased hydrodynamic power motivates the adsorption of nanosheets, and the climbing film is constructed by the abundant adsorption of JGO-5. This is ascribed to the weak interaction among the JGO-5 at the interface, thus the preferentially adsorbed JGO-5 will be pushed to
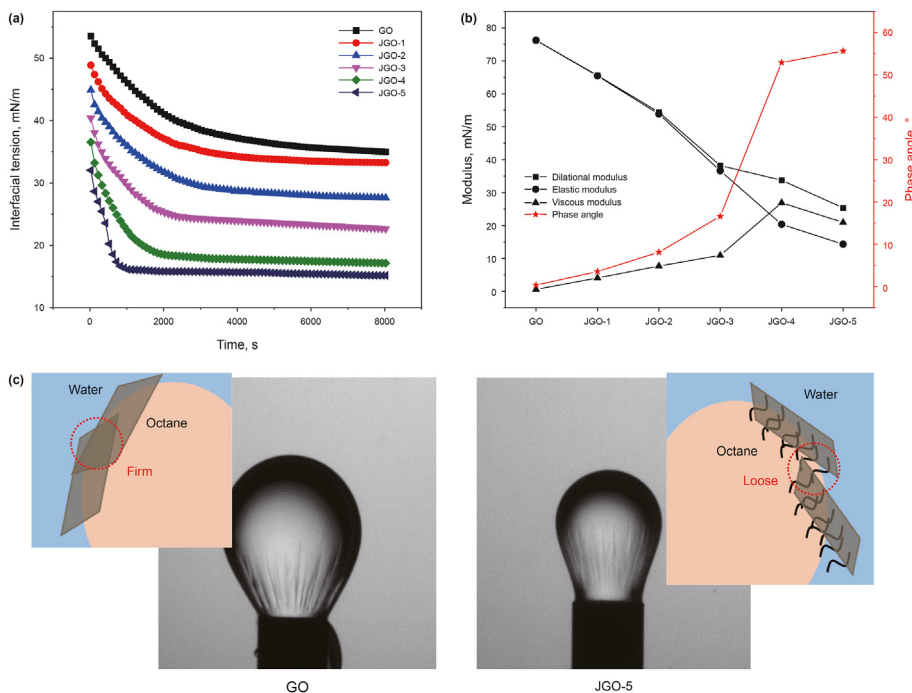

Fig. 3. Interfacial properties of GO/JGO. (**a**) Interfacial tension between octane and sample aqueous solutions; (**b**) Dilatational interfacial rheology of GO and JGO at the octane-water interface; (**c**) Drop images in the dilatational experiments of GO and JGO-5 after compression and the schematic of the interfacial films of GO and JGO at the octane-water interface.
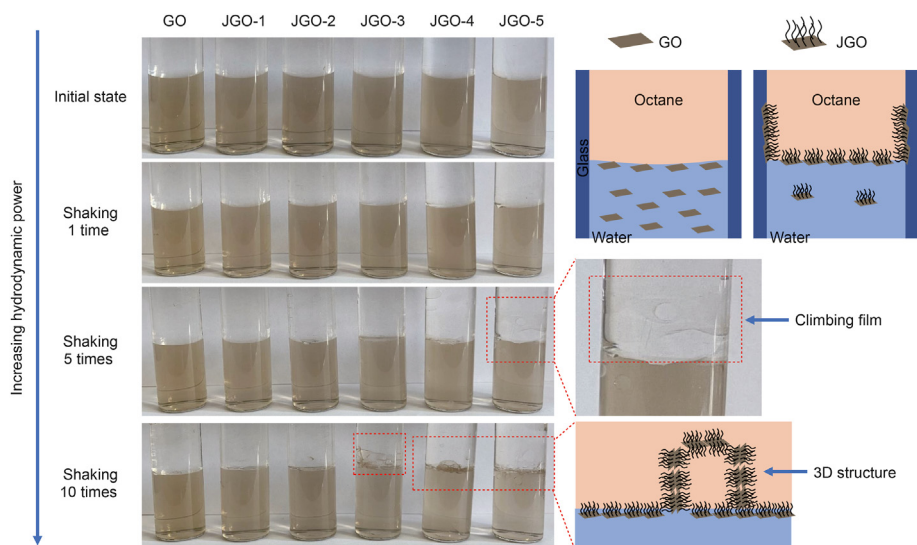
Fig. 4. Adsorption of GO and JGO with different modification degrees at the octane-water interface with increasing hydrodynamic power.

the oil-glass interface to provide space for the subsequent adsorption of JGO-5. Further increasing the hydrodynamic power, JGO-3 also fabricates the climbing film. Meanwhile, the bilayer or 3D structures are constructed at the interface due to the massive adsorption of JGO-4 and JGO-5. However, GO cannot fabricate the climbing film due to its high affinity to water. It is believed that JGO with higher modification degrees can construct the climbing film under appropriate hydrodynamic power, which is critical for its performance in EOR process.

Apart from the liquid-liquid interface, the impact of modification degrees on the property of JGO at the solid-liquid interface is also explored (Fig. 5). The initial oil contact angle (IOCA) of the sandstone slab immersed in the GO solution is 13.0°, reflecting the strong oil-wet surface of sandstone slab after aged in crude oil. After immersed for 48 h, the final oil contact angle (FOCA) increases to 37.5°, which should be attributed to the adsorption of GO with slight amphiphilicity at the rock surface. For sandstone slabs immersed in JGO solutions, the slabs become more hydrophilic from JGO-1 to JGO-5, with the IOCA increasing from 17.3° to 43.5° and the FOCA increasing from 37.5° to 125.8°. The Janus structure of JGO might be responsible for their great wettability alteration ability. The hydrophobic interaction between the dodecylamine modified side of JGO and the organic materials initially adsorbed at the rock surface promotes the adsorption of JGO at the oil-wet surface, which can be facilitated by higher modification degrees of JGO. Thus, the hydrophilic side on JGO with higher modification

degrees can cover the oil-wet rock surface more effectively to achieve the wettability alteration.

3.3. Effects of modification degrees on the EOR efficiency of JGO

The above results demonstrate that the modification degrees of JGO significantly impact their interfacial activity at both liquid-liquid and liquid-solid interface, which is critical for the EOR application of JGO. Then, core flooding tests are conducted to further specify the EOR efficiency of JGO with different modification degrees. The results are summarized in Table 2 and Fig. 6. It should be pointed out that the soak time is 12 h after the injection of nanofluids, which is essential for the formation of interfacial films (Fig. 4).

The recovery after first water flooding (FWF) in all experiments is in the range between 61.05% and 64.62% due to the similar physical parameters of these cores. During the injection of GO solution, the recovery is only improved by 2.5%, and further improved by 0.83% after chase water flooding (CWF). As shown in Fig. S4, JGO exhibits the greater ability to reduce the water/crude oil interfacial tension with the increase of modification degrees. Meanwhile, the interfacial tension of crude oil system is higher than that of the simulated oil system (Fig. 3a), which is ascribed to the complex components of crude oil (Pal and Mandal, 2020b). The improvement of oil recovery after the JGO nanofluids flooding (NFF) gradually raises with the increased modification degrees, which should
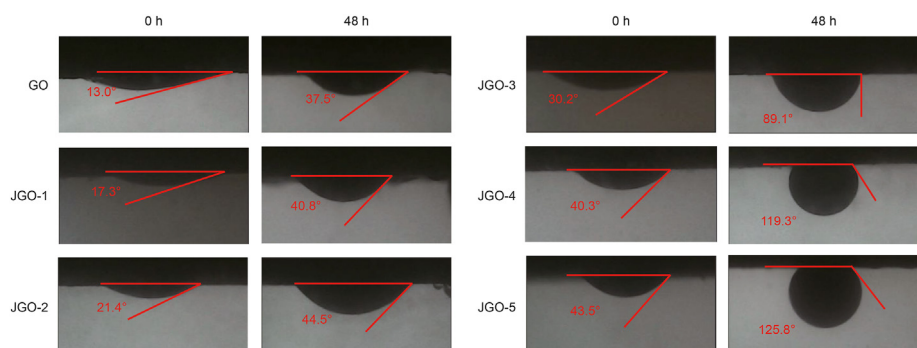

Fig. 5. The contact angle of oil-wet sandstone slab immersed in sample aqueous solutions (50 mg/L) toward crude oil.

Table 2
Results of core flooding tests.

No.	Nanofluids	Recovery, %				
		After water flooding	After nanofluids flooding	After chase water flooding	Improved by nanofluids	Improved by chase water
a	GO	63.33	65.83	66.67	2.50	0.83
b	JGO-1	63.29	65.82	68.61	2.53	2.79
c	JGO-2	64.62	68.00	71.08	3.38	3.08
d	JGO-3	61.44	66.67	71.90	5.23	5.23
e	JGO-4	62.89	68.19	74.46	5.30	6.27
f	JGO-5	63.15	68.40	73.24	5.25	4.84
g	JGO-2	64.62	70.00	76.15	5.38	6.15
h	JGO-2	61.05	64.05	65.10	3.00	1.05
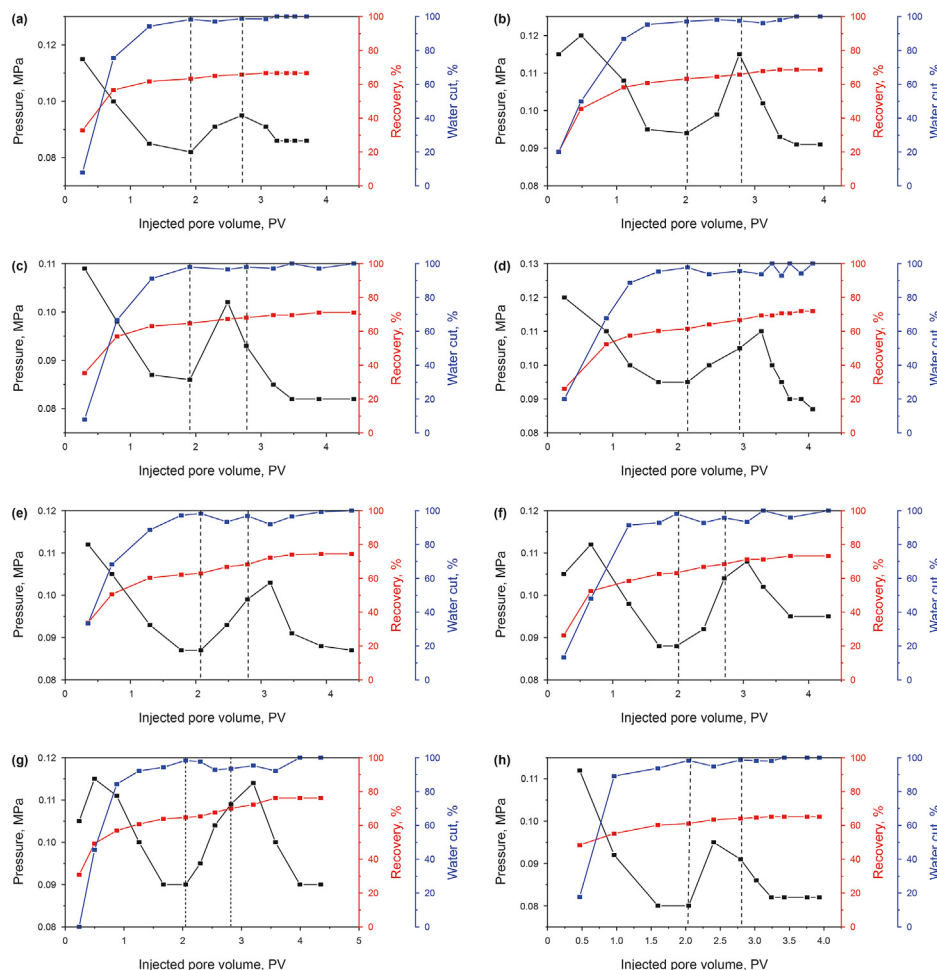
Fig. 6. Results of core flooding tests using different sample nanofluids. (**a**) GO; (**b**) JGO-1; (**c**) JGO-2; (**d**) JGO-3; (**e**) JGO-4; (**f**) JGO-5; (**g**) nanofluid is JGO-2 and the injection rate during NFF stage is 0.3 mL/min; (**h**) nanofluid is JGO-2 and the CWF starts right after the NFF.

be attributed to their enhanced interfacial activity (Fig. 3a) and wettability alteration ability (Fig. 5). Furthermore, the CWF is much more effective in the JGO involved tests, especially the best performance (6.27%) of JGO-4. It is speculated that the remarkable efficiency of CWF in the presence of JGO might be related to the formation of interfacial films and climbing films. In the stage of CWF, the formed interfacial film can push the oil slug to the outlet, and the climbing film may insert in to the space between oil and rock surface, detaching the oil from the rock surface (Jeon et al., 2019; Luo et al., 2016). As discussed above, JGO with higher modification degrees easily construct interfacial and climbing films (Fig. 4), so the efficiency of CWF is gradually increased from JGO-1

to JGO-4. JGO-5 may form 3D structures at the oil-water interface under such hydrodynamic power to plug some pores and reduce the flow channel for oil, which may be responsible for its reduced EOR efficiency (4.84%) at the CWF stage.

The pressure variation during the displacement process (Fig. 6) can provide more insights into the EOR mechanism of JGO. During the NFF, the injection pressure in all experiments rises in different degrees, which is due to the enhanced flow resistance caused by the nanosheets. In the CWF stage of GO involved test, the pressure drops instantly and the final pressure (P_{CWF}) exceeds the pressure (P_{FWF}) after the FWF, reflecting no interfacial films formed by GO. The similar phenomenon is also observed in JGO-1 and JGO-2

involved tests that the pressure drops immediately at the beginning of CWF, whereas the P_{CWF} is lower than P_{FWF}. The lower pressure means the rock surface becomes more hydrophobic to reduce the resistance of rock surface to water. It is demonstrated that the JGO exhibits the great ability to change hydrophilic surface to hydrophobic surface (Fig. S2). Then, the JGO might be effective for EOR in the aspect of step-down augmented injection. In the experiments of JGO-3 and JGO-4, the pressure gradually builds up in the CWF process, which should be attributed to the well-constructed interfacial films. Nevertheless, the P_{CWF} in the two experiments is no greater than P_{FWF} due to the superior wettability alteration ability of JGO-3 and JGO-4. For JGO-5, it is worth noting that the P_{CWF} is larger than P_{FWF}, which might be attributed to the more dominant plugging effects of the formed 3D structures at oil-water interface than the wettability alteration of JGO-5. The pressure variation further confirms the proposed EOR mechanism of JGO and reveals the potential of JGO as "smart" wettability alteration agent.

It is believed that the ability of JGO to construct interfacial films, climbing films, and alter the wettability of rock surface is critical to its remarkable performance in EOR. The intensity of hydrodynamic power is another critical factor to facilitate the formation of JGO interfacial films. Therefore, the impact of hydrodynamic power on the EOR efficiency of JGO is further investigated. In the control experiment used JGO-2 with the relatively low modification degree, the change of hydrodynamic power is achieved by increasing the injection rate of nanofluids from 0.2 mL/min to 0.3 mL/min. As shown in Table 2 and Fig. 6, similar recovery is obtained after water flooding. Compared with the improved oil recovery (3.38%) in JGO-2 system at low injection rate, the higher flow rate moderately increases the oil recovery to 5.38%. Besides, the pressure rises at the beginning of CWF and the greater P_{CWF} than P_{FWF} are closely related to the interface film and the 3D structure of JGO-2, respectively. More importantly, the recovery enhancement after the CWF stage increases from 3.08% to 6.15%, although the injection rate keeps the same. It is concluded that rising the injection rate can be an effective way to improve the EOR performance of JGO with lower modification degrees. Correspondingly, the injection rate of JGO with higher modification degrees should be carefully controlled to avoid the blocking of flow channels. In the other control experiment used JGO-2 nanofluids, the CWF starts immediately after NFF without soaking (Fig. 6h). The much lower recovery in the stage of CWF in this test directly verifies the extreme necessity of soaking for the EOR performance of JGO.

4. Conclusions

In this study, we synthesized a series of dodecylamine grafted JGO with different modification degrees and evaluated their interfacial properties and EOR performances. It is found that JGO shows the great oil-water interfacial activity (large IFT reduction and low dilatational modulus) to generate 2D interfacial films and 3D climbing films, which can be evidently improved by increased modification degrees and enhanced hydrodynamic power. Moreover, the JGO-5 with higher modification degree exhibits superior wettability alteration efficiency at the liquid-solid interface. Both the generation of climbing films and the great ability of wettability alteration can improve the insertion of JGO to the space between oil and rock surface and effectively detach the oil from the rock surface, which is verified via the core flooding tests. The variations of the injection pressure reflect the JGO with high modification degrees can easily fabricate 3D structures to block the flow channels, and the JGO with moderate modification degrees are more suitable for the EOR application with carefully controlled injection rate. The present study provides novel insights to the microscopic EOR mechanism of alkylamine modified JGO with different modification

degrees, which is highly essential for the practical application of JGO in EOR.

Declaration of competing interest

The authors declare that they have no known competing financial interests or personal relationships that could have appeared to influence the work reported in this paper.

Appendix A. Supplementary data

Supplementary data to this article can be found online at https://doi.org/10.1016/j.petsci.2022.08.032.

References

Al-Anssari, S., Barifcani, A., Wang, S.B., Maxim, L., Iglauer, S., 2016. Wettability alteration of oil-wet carbonate by silica nanofluid. J. Colloid Interface Sci. 461, 435–442. https://doi.org/10.1016/j.jcis.2015.09.051.

Al-Anssari, S., Wang, S.B., Barifcani, A., Lebedev, M., Iglauer, S., 2017. Effect of temperature and SiO2 nanoparticle size on wettability alteration of oil-wet calcite. Fuel 206, 34–42. https://doi.org/10.1016/j.fuel.2017.05.077.

Ali, M., Aftab, A., Awan, F.U.R., Akhondzadeh, H., Keshavarz, A., Saeedi, A., Iglauer, S., Sarmadivaleh, M., 2021. CO2-wettability reversal of cap-rock by alumina nanofluid: implications for CO2 geo-storage. Fuel Process. Technol. 214, 11. https://doi.org/10.1016/j.fuproc.2021.106722.

Ali, M., Sahito, M.F., Jha, N.K., Arain, Z.U.A., Memon, S., Keshavarz, A., Iglauer, S., Saeedi, A., Sarmadivaleh, M., 2020. Effect of nanofluid on CO2-wettability reversal of sandstone formation; implications for CO2 geo-storage. J. Colloid Interface Sci. 559, 304–312. https://doi.org/10.1016/j.jcis.2019.10.028.

Alnarabiji, M.S., Yahya, N., Nadeem, S., Adil, M., Baig, M.K., Ben Ghanem, O., Azizi, K., Ahmed, S., Maulianda, B., Klemes, J.J., Elraies, K.A., 2018. Nanofluid enhanced oil recovery using induced ZnO nanocrystals by electromagnetic energy: viscosity increment. Fuel 233, 632–643. https://doi.org/10.1016/j.fuel.2018.06.068.

Barrabino, A., Holt, T., Lindeberg, E., 2018. An evaluation of graphene oxides as possible foam stabilizing agents for CO2 based enhanced oil recovery. Nanomaterials 8 (8), 12. https://doi.org/10.3390/nano8080603.

Cao, J., Chen, Y.P., Zhang, J., Wang, X.J., Wang, J., Shi, C.X., Ning, Y.F., Wang, X.M., 2022. Preparation and application of nanofluid flooding based on polyoxyethylated graphene oxide nanosheets for enhanced oil recovery. Chem. Eng. Sci. 247, 11. https://doi.org/10.1016/j.ces.2021.117023.

Chen, L.H., Wei, J., Tian, Q., Han, Z.C., Li, L., Meng, S.J., Hasi, Q.M., 2021. Dual-Functional graphene oxide-based photothermal materials with aligned channels and oleophobicity for efficient solar steam generation. Langmuir 37 (33), 10191–10199. https://doi.org/10.1021/acs.langmuir.1c01647.

de Vasconcelos, C.K.B., Medeiros, F.S., Diniz, B.R.S., Viana, M.M., Caliman, V., Silva, G.G., 2022. Nanofluids based on hydrolyzed polyacrylamide and aminated graphene oxide for enhanced oil recovery in different reservoir conditions. Fuel 310, 10. https://doi.org/10.1016/j.fuel.2021.122299.

Dimiev, A.M., Tour, J.M., 2014. Mechanism of graphene oxide formation. ACS Nano 8 (3), 3060–3068. https://doi.org/10.1021/nn500606a.

Dreyer, D.R., Park, S., Bielawski, C.W., Ruoff, R.S., 2010. The chemistry of graphene oxide. Chem. Soc. Rev. 39 (1), 228–240. https://doi.org/10.1039/b917103g.

Fang, S.W., Chen, T., Chen, B., Xiong, Y., Zhu, Y., Duan, M., 2016. Graphene oxide at oil-water interfaces: adsorption, assembly & demulsification. Colloids Surf. A Physicochem. Eng. Asp. 511, 47–54. https://doi.org/10.1016/j.colsurfa.2016.09.058.

Giraldo, L.J., Gallego, J., Villegas, J.P., Franco, C.A., Cortes, F.B., 2019. Enhanced waterflooding with NiO/SiO2 0-D Janus nanoparticles at low concentration. J. Petrol. Sci. Eng. 174, 40–48. https://doi.org/10.1016/j.petrol.2018.11.007.

Huang, P., Jia, H., Wang, T.Y., Xu, Y.B., Zhang, L.Y., Wei, X., Jia, H.D., Wen, S.J., Lv, K.H., Liu, D.X., 2021. Effects of modification degrees on the colloidal stability of amphiphilic Janus graphene oxide in aqueous solution with and without electrolytes. Langmuir 37 (33), 10061–10070. https://doi.org/10.1021/acs.langmuir.1c01283.

Jafarbeigi, E., Kamari, E., Salimi, F., Mohammadidoust, A., 2020. Experimental study of the effects of a novel nanoparticle on enhanced oil recovery in carbonate porous media. J. Petrol. Sci. Eng. 195, 12. https://doi.org/10.1016/j.petrol.2020.107602.

Jeon, I., Peeks, M.D., Savagatrup, S., Zeininger, L., Chang, S., Thomas, G., Wang, W., Swager, T.M., 2019. Janus graphene: scalable self-assembly and solution-phase

orthogonal functionalization. Adv. Mater. 31 (21), 7. https://doi.org/10.1002/adma.201900438.

Jia, C.Q., Huang, Z.Q., Sepehrnoori, K., Yao, J., 2021a. Modification of two-scale continuum model and numerical studies for carbonate matrix acidizing. J. Petrol. Sci. Eng. 197. https://doi.org/10.1016/j.petrol.2020.107972.

Jia, C.Q., Sepehrnoori, K., Huang, Z.Q., Yao, J., 2021b. Modeling and analysis of carbonate matrix acidizing using a new two-scale continuum model. SPE J. 26 (5), 2570—2599.

Kovalchuk, V.I., Aksenenko, E.V., Makievski, A.V., Fainerman, V.B., Miller, R., 2019. Dilational interfacial rheology of tridecyl dimethyl phosphine oxide adsorption layers at the water/hexane interface. J. Colloid Interface Sci. 539, 30—37. https://doi.org/10.1016/j.jcis.2018.12.019.

Kumar, R., Sahoo, S., Joanni, E., Singh, R.K., Tan, W.K., Kar, K.K., Matsuda, A., 2019. Recent progress in the synthesis of graphene and derived materials for next generation electrodes of high performance lithium ion batteries. Prog. Energy Combust. Sci. 75, 56. https://doi.org/10.1016/j.pecs.2019.100786.

Li, W.J., Tang, X.Z., Zhang, H.B., Jiang, Z.G., Yu, Z.Z., Du, X.S., Mai, Y.W., 2011. Simultaneous surface functionalization and reduction of graphene oxide with octadecylamine for electrically conductive polystyrene composites. Carbon 49 (14), 4724—4730. https://doi.org/10.1016/j.carbon.2011.06.077.

Liu, J., Li, X.C., Jia, W.H., Li, Z.Y., Zhao, Y.P., Ren, S.L., 2015. Demulsification of crude oil-in-water emulsions driven by graphene oxide nanosheets. Energy Fuel. 29 (7), 4644—4653. https://doi.org/10.1021/acs.energyfuels.5b00966.

Liu, W.S., Koh, K.L., Lu, J.L., Yang, L.P., Phua, S.L., Kong, J.H., Chen, Z., Lu, X.H., 2012. Simultaneous catalyzing and reinforcing effects of imidazole-functionalized graphene in anhydride-cured epoxies. J. Mater. Chem. 22 (35), 18395—18402. https://doi.org/10.1039/c2jm32708b.

Lonkar, S.P., Deshmukh, Y.S., Abdala, A.A., 2015. Recent advances in chemical modifications of graphene. Nano Res. 8 (4), 1039—1074. https://doi.org/10.1007/s12274-014-0622-9.

Luo, D., Wang, F., Zhu, J.Y., Cao, F., Liu, Y., Li, X.G., Willson, R.C., Yang, Z.Z., Chu, C.W., Ren, Z.F., 2016. Nanofluid of graphene-based amphiphilic Janus nanosheets for tertiary or enhanced oil recovery: high performance at low concentration. Proc. Natl. Acad. Sci. U. S. A 113 (28), 7711—7716. https://doi.org/10.1073/pnas.1608135113.

Luo, D., Wang, F., Zhu, J.Y., Tang, L., Zhu, Z., Bao, J.M., Willson, R.C., Yang, Z.Z., Ren, Z.F., 2017. Secondary oil recovery using graphene-based amphiphilic Janus nanosheet fluid at an ultralow concentration. Ind. Eng. Chem. Res. 56 (39), 11125—11132. https://doi.org/10.1021/acs.iecr.7b02384.

Lv, K.H., Huang, P., Zhou, Z.S., Wei, X., Luo, Q., Huang, Z.M., Yan, H., Jia, H., 2020. Study of Janus amphiphilic graphene oxide as a high-performance shale inhibitor and its inhibition mechanism. Front. Chem. 8, 9. https://doi.org/10.3389/fchem.2020.00201.

Maurya, N.K., Kushwaha, P., Mandal, A., 2017. Studies on interfacial and rheological properties of water soluble polymer grafted nanoparticle for application in enhanced oil recovery. J. Taiwan Inst. Chem. Eng. 70, 319—330. https://doi.org/10.1016/j.jtice.2016.10.021.

Maurya, N.K., Mandal, A., 2016. Studies on behavior of suspension of silica nanoparticle in aqueous polyacrylamide solution for application in enhanced oil recovery. Petrol. Sci. Technol. 34 (5), 429—436. https://doi.org/10.1080/10916466.2016.1145693.

Maurya, N.K., Mandal, A., 2018. Investigation of synergistic effect of nanoparticle and surfactant in macro emulsion based EOR application in oil reservoirs. Chem. Eng. Res. Des. 132, 370—384. https://doi.org/10.1016/j.cherd.2018.01.049.

Ng, S.W., Noor, N., Zheng, Z.J., 2018. Graphene-based two-dimensional Janus materials. NPG Asia Mater. 10, 21. https://doi.org/10.1038/s41427-018-0023-8.

Pal, N., Mandal, A., 2020a. Enhanced oil recovery performance of gemini surfactant-stabilized nanoemulsions functionalized with partially hydrolyzed polymer/silica nanoparticles. Chem. Eng. Sci. 226. https://doi.org/10.1016/j.ces.2020.115887.

Pal, N., Mandal, A., 2020b. Oil recovery mechanisms of Pickering nanoemulsions stabilized by surfactant-polymer-nanoparticle assemblies: a versatile surface energies' approach. Fuel 276. https://doi.org/10.1016/j.fuel.2020.118138.

Pei, J.Y., Zhao, H.Y., Yang, F., Yan, D., 2021. Graphene oxide/Fe₂O₃ nanocomposite as an efficient catalyst for thermal decomposition of ammonium perchlorate via the vacuum-freeze-drying method. Langmuir 37 (20), 6132—6138. https://doi.org/10.1021/acs.langmuir.1c00108.

Periasamy, A.P., Wu, W.P., Ravindranath, R., Roy, P., Lin, G.L., Chang, H.T., 2017. Polymer/reduced graphene functionalized sponges as superabsorbents for oil removal and recovery. Mar. Pollut. Bull. 114 (2), 888—895. https://doi.org/10.1016/j.marpolbul.2016.11.005.

Shamaila, S., Sajjad, A.K.L., Iqbal, A., 2016. Modifications in development of graphene oxide synthetic routes. Chem. Eng. J. 294, 458—477. https://doi.org/10.1016/j.cej.2016.02.109.

Shams, M., Guiney, L.M., Huang, L.J., Ramesh, M., Yang, X.N., Hersam, M.C., Chowdhury, I., 2019. Influence of functional groups on the degradation of

graphene oxide nanomaterials. Environ. Sci. Nano. 6 (7), 2203—2214. https://doi.org/10.1039/c9en00355j.

Sherlala, A.I.A., Raman, A.A.A., Bello, M.M., Asghar, A., 2018. A review of the applications of organo-functionalized magnetic graphene oxide nanocomposites for heavy metal adsorption. Chemosphere 193, 1004—1017. https://doi.org/10.1016/j.chemosphere.2017.11.093.

Sikiru, S., Rostami, A., Soleimani, H., Yahya, N., Afeez, Y., Aliu, O., Yusuf, J.Y., Oladosu, T.L., 2021. Graphene: outlook in the enhance oil recovery (EOR). J. Mol. Liq. 321, 13. https://doi.org/10.1016/j.molliq.2020.114519.

Suleimanov, B.A., Ismailov, F.S., Veliyev, E.F., 2011. Nanofluid for enhanced oil recovery. J. Petrol. Sci. Eng. 78 (2), 431—437. https://doi.org/10.1016/j.petrol.2011.06.014.

Sun, X.F., Zhang, Y.Y., Chen, G.P., Gai, Z.Y., 2017. Application of nanoparticles in enhanced oil recovery: a critical review of recent progress. Energies 10 (3), 33. https://doi.org/10.3390/en10030345.

Tadjarodi, A., Ferdowsi, S.M., Zare-Dorabei, R., Barzin, A., 2016. Highly efficient ultrasonic-assisted removal of Hg(II) ions on graphene oxide modified with 2-pyridinecarboxaldehyde thiosemicarbazone: adsorption isotherms and kinetics studies. Ultrason. Sonochem. 33, 118—128. https://doi.org/10.1016/j.ultsonch.2016.04.030.

Tian, Y.H., Yu, Z.C., Cao, L.Y., Zhang, X.L., Sun, C.H., Wang, D.W., 2021. Graphene oxide: an emerging electromaterial for energy storage and conversion. J. Energy Chem. 55, 323—344. https://doi.org/10.1016/j.jechem.2020.07.006.

Toda, K., Furue, R., Hayami, S., 2015. Recent progress in applications of graphene oxide for gas sensing: a review. Anal. Chim. Acta 878, 43—53. https://doi.org/10.1016/j.aca.2015.02.002.

Tohidi, Z., Teimouri, A., Gharibshahi, R., Omidkhah, M.R., 2022. Application of Janus nanoparticles in enhanced oil recovery processes: current status and future opportunities. J. Petrol. Sci. Eng. 208, 12. https://doi.org/10.1016/j.petrol.2021.109602.

Wang, Y., Li, S.S., Yang, H.Y., Luo, J., 2020. Progress in the functional modification of graphene/graphene oxide: a review. RSC Adv. 10 (26), 15328—15345. https://doi.org/10.1039/d0ra01068e.

Wang, Z.H., Ge, Z.L., Zheng, X.X., Chen, N., Peng, C., Fan, C.H., Huang, Q., 2012. Polyvalent DNA-graphene nanosheets "click" conjugates. Nanoscale 4 (2), 394—399. https://doi.org/10.1039/c1nr11174d.

Wei, B., Li, H., Li, Q.Z., Wen, Y.B., Sun, L., Wei, P., Pu, W.F., Li, Y.B., 2017. Stabilization of foam lamella using novel surface-grafted nanocellulose-based nanofluids. Langmuir 33 (21), 5127—5139. https://doi.org/10.1021/acs.langmuir.7b00387.

Wu, H., Yi, W.Y., Chen, Z., Wang, H.T., Du, Q.G., 2015. Janus graphene oxide nanosheets prepared via Pickering emulsion template. Carbon 93, 473—483. https://doi.org/10.1016/j.carbon.2015.05.083.

Xiao, L.Q., Liao, L.Q., Liu, L.J., 2013. Chemical modification of graphene oxide with carbethoxycarbene under microwave irradiation. Chem. Phys. Lett. 556, 376—379. https://doi.org/10.1016/j.cplett.2012.11.084.

Yin, T.H., Yang, Z.H., Dong, Z.X., Lin, M.Q., Zhang, J., 2019. Physicochemical properties and potential applications of silica-based amphiphilic Janus nanosheets for enhanced oil recovery. Fuel 237, 344—351. https://doi.org/10.1016/j.fuel.2018.10.028.

Yoon, K.Y., An, S.J., Chen, Y.S., Lee, J.H., Bryant, S.L., Ruoff, R.S., Huh, C., Johnston, K.P., 2013. Graphene oxide nanoplatelet dispersions in concentrated NaCl and stabilization of oil/water emulsions. J. Colloid Interface Sci. 403, 1—6. https://doi.org/10.1016/j.jcis.2013.03.012.

Zeng, L.L., Zhang, Z.J., Qiu, W.J., Wei, J.K., Fang, Z.H., Deng, Q.B., Guo, W., Liu, D., Xie, Z.Z., Qu, D.Y., Tang, H.L., Li, J.S., Hu, N., 2020. Multifunctional polypropylene separator via cooperative modification and its application in the lithium-sulfur battery. Langmuir 36 (37), 11147—11153. https://doi.org/10.1021/acs.langmuir.0c02216.

Zhang, H., Ramakrishnan, T.S., Nikolov, A., Wasan, D., 2018. Enhanced oil displacement by nanofluid's structural disjoining pressure in model fractured porous media. J. Colloid Interface Sci. 511, 48—56. https://doi.org/10.1016/j.jcis.2017.09.067.

Zhang, J., Chen, L.Q., Chen, J.D., Zhang, Q., Feng, J., 2019. Stability, cellular uptake, and in vivo tracking of zwitterion modified graphene oxide as a drug carrier. Langmuir 35 (5), 1495—1502. https://doi.org/10.1021/acs.langmuir.8b01995.

Zhang, W.Q., Wang, Z.H., Lv, S.D., Zhan, W.W., Bai, G., Zhou, A.S., Sui, G., Yang, X.P., 2021. Molecular simulation of different structure dopamine-modified graphene oxide and its effects on thermal and mechanical properties of the epoxy resin system. Polymer 212, 9. https://doi.org/10.1016/j.polymer.2020.123120.

Zhang, Z., An, Y.X., 2018. Nanotechnology for the oil and gas industry - an overview of recent progress. Nanotechnol. Rev. 7 (4), 341—353. https://doi.org/10.1515/ntrev-2018-0061.

Zhao, M.W., Lv, W.J., Li, Y.Y., Dai, C.L., Wang, X.K., Zhou, H.D., Zou, C.W., Gao, M.W., Zhang, Y., Wu, Y.N., 2018. Study on the synergy between silica nanoparticles and surfactants for enhanced oil recovery during spontaneous imbibition. J. Mol. Liq. 261, 373—378. https://doi.org/10.1016/j.molliq.2018.04.034.